Iranian Journal of Medical Physics

ijmp.mums.ac.ir

Radiation Dose Optimization during Temporal Bone CT Examination Using One-Shot Axial Volumetric Acquisition

Youssef Madkouri[1], Mohammed. Aggour[1], Youssef Bouzekraoui[2*], Farida Bentayeb[3]

1. Laboratory of Electronic Systems, Information Processing, Mechanics and Energetics, Faculty of Sciences, University Ibn Tofail Kenitra, Morocco
2. Hassan First University of Settat, High Institute of Health Sciences, Laboratory of Sciences and Health Technologies, Settat, Morocco
3. Department of Physics, LPHE, Modeling and Simulations, Faculty of Science, Mohammed V University, Rabat, Morocco

ARTICLE INFO

Article type:
Original Paper

Article history:
Received: Feb 10, 2022
Accepted: Jul 27, 2022

Keywords:
Computed Tomography
Volumetric
Temporal Bone

ABSTRACT

Introduction: The optimization of radiation exposure when exploring small and complex anatomical structures is the most important issue for temporal bone CT. The objective of this study is to use single-shot volume acquisition in order to minimize the dose and compare the obtained image quality to a conventional helical technique.

Material and Methods: Twenty patients (8 males, 12 females) were scanned using the 135kVp single-shot volume mode (VMCT135-kVp) whereas other twenty patients (9 males, 11 females) were examined using the 120kVp helical mode (HMCT120-kVp). A physician-interpreter evaluated the subjective conspicuity of 53 structures in the temporal bone on a 5-point scale using multiplanar reconstruction (MPR). In addition, the image noise in both techniques was quantified by analyzing it in three different regions of interest (ROIs). Radiation dose reduction was noted and compared with literature-based effective dose dosimetry data.

Results: The mean dose-length-product (DLP) for the VMCT135-kVp was (69.6±2.5 mGy.cm), which was significantly lower ($p<0.001$), compared to (186.4±4.3 mGy.cm) for HMCT120-kVp. Similarly, the effective dose (0.15±0.01 mSv) for VMCT135-kVp was reduced by approximately 61.5% relative to (0.39±0.05 mSv) for HMCT120-kVp. In contrast, there was no significant difference in the image noise average between the two protocols ($p> 0.05$). Indeed, the overall analysis of the 53 anatomic structures revealed no differences between the two protocols, and most anatomic structures were identified.

Conclusion: For temporal bone, the VMCT135-kVp scan significantly reduces radiation exposure compared to the HMCT120-kVp. The obtained dose was lower compared to the literature-based protocol while maintaining image visualization quality.

►*Please cite this article as:*
Madkouri Y, Aggour M, Bouzekraoui Y, Bentayeb F. Radiation Dose Optimization during Temporal Bone CT Examination Using One-Shot Axial Volumetric Acquisition . Iran J Med Phys 2023; 20: 215-221.10.22038/IJMP.2022.63627.2087.

Introduction

The human ear is divided into three parts: the outer ear is the only visible part, and the middle ear and the inner ear are included in the temporal bone. The temporal bone is a complex and crucial anatomical structure, the seat of the otic capsule, responsible for the hearing and balance mechanism [1]. This organ is composed of bone and air of the outer and middle ear, bone, and fluid for the inner ear. Density variations in those parts are extreme and show the largest difference in the Hounsfield scale, for this reason, CT scan without injection of iodinated contrast is the reference examination to study the temporal bone organ but is not typical, intravenous contrast should be used in some specific cases, such as vascular tumors or otomastoiditis [2]. The CT exam may be supplemented by magnetic resonance imaging (most often performed by injection) to study the soft tissue and fluid structures of the inner ear [3]. The temporal bone scan is a valuable method for diagnosing inflammatory pathologies of the ear and evaluating surgical procedures [4]. This examination is mainly prescribed in the following cases: hearing impairment, balance disorders, peripheral facial paralysis, ear pain, otitis, otosclerosis, cholesteatoma, infectious pathology, control after surgery and tumors [1, 5-7].

For all areas of the body, the most important point and diagnostic task of CT imaging are to ensure the highest image quality at the lowest possible dose [8]. With the helical mode, in order to ensure that the first and last slices of the acquisition are complete, it is necessary to make an additional turn at the start and at the end of the helical acquisition which is located outside the explored zone, the present operation is needed for data reconstruction interpolation. This "pre- and post-helix" exposure is called overranging or z-overscanning. The percentage of dose induced by overranging is inversely proportional to the length of the explored volume [9]. As a result, with CT scanners, overranging can represent a considerable

*Corresponding Author: Tel: +212623609312; Email: youssef0fsr@gmail.com

part of the total irradiation (around 10% for CT abdominal and up to 20 or 30 % for CT cardiac acquisition) [10]. The so-called overbeaming effect in the helical configuration causes overdosing at the penumbra region which is not useful for data image reconstruction and thus only contributes to an excess of radiation exposure [11-12].

To achieve a low dose by reducing the radiation exposure time in the temporal bone region, the volumetric acquisition technique can be used instead of the helical acquisition technique [13]. First, The CT volume scanning mode consists in a single rotation of the gantry without moving the table, which also reduces the scanning time [14]. Second, this method reduces penumbra or overbeaming phenomena, and inherently lack of z-axis overranging, compared to the helical scan mode [15].

X-ray exposure in the medical field requires special attention to patients and staff radiation protection. Since this is important in CT examinations to avoid risk of developing leukemia and brain tumors for children and adolescents [16] , this work was concerned with optimizing the delivered dose in addition to image quality. An investigation and analysis of the image quality as well as the delivered dose has been performed for the two protocols used: One-shot volume scanning mode computed tomography with a single tube rotation at 135kVp (VMCT135-kVp) and the conventional helical scanning mode computed tomography at 120kVp (HMCT120-kVp).

Materials and Methods

Patient selection and techniques of CT acquisition

From January to November 2019, we followed 40 patients (17 males, 23 females) for this study; all of them are trauma and tumor free. Among them, 20 patients acquisitions were performed using the HMCT120-kVp protocol, and 20 other patients were selected for the VMCT135-kVp protocol. Concerning the volume scan mode at 135 kVp and 75mAs, 4 cm of volume scan in one rotation with a scan time of 0.5 second (without pitch) is acquired using 80 sections. For the helical mode at 120 kVp and 100 mAs, we used a collimation of 0.5 × 80- row, a pitch of 0.65, a scan time of 1.42 second and a scan range of 40 mm. All protocols were acquired by iterative reconstruction using Adaptive Iterative Dose Reduction three Dimension (AIDR 3D, CT Prime 80-Row, Toshiba Medical System, Otawara, Japan) and Filter Back Projection Kernel (FC 81). The thickness of the reconstructed slice is 0.5 mm and the reconstruction interval is 0.25 mm. All images were displayed at bone window (800 Hounsfield Units (HU) for the window center and 4500 HU for the window width).The resolution of images matrix in figures 1 and 2 is 1,024 × 1,024 in a display monitor (display console, version 4.74, Toshiba Medical System, Otawara, Japan).

Dose evaluation

The delivered dose was provided by the examination report. Depending on the conditions and the scanning mode, the Computed Tomographic Dose Index volume (CTDIvol) and Dose Length Product (DLP) are calculated as described below:

-Volume scan mode

The dependence between $CTDI_{vol}$, DLP and $CTDI_w$ values are described by the following equations:

$$CTDI_{VOL} = CTDI_W . R \quad (1)$$

$$DLP = CTDI_{VOL} . N . T \quad (2)$$

Where CTDIW is a weighted average dose across a single slice [17], R is the number of rotations, N is the number of scanned slices per rotation and T is the scan slice thickness in centimeters.

-Helical scan mode

The relation-ship between $CTDI_{vol}$, DLP and $CTDI_w$ values is given by:

$$CTDI_{VOL} CTDI_W . N . \frac{T}{M} \quad (3)$$

$$DLP = CTDI_{VOL} . L \quad (4)$$

Where N is the number of scanned slices per rotation, T is the slice thickness in centimeters, M is the couch movement distance in centimeters per rotation, and L is the helical scan range in centimeters.

The effective dose, E, was calculated by multiplying the DLP with the region-specific normalized effective dose conversion factor 0.0031 [mSv/(mGy.cm)] for the head and neck region (including the temporal bone) as follows:[18]

$$E = K . DLP \ (mSv) \quad (5)$$

Where K is the region-specific normalized effective dose conversion factor.

Qualitative and quantitative analysis of image quality

Image quality was evaluated qualitatively and quantitatively using the native 0.5 mm axial section. The examinations were reviewed from a CT scan Toshiba Aquilion Prime post-processing console, using multiplanar reconstruction (MPR) and bone window. For the qualitative analysis, a radiologist in CT imaging ,with 30 years of experience, evaluated 53 temporal bone anatomical structures using different protocols [19-20], based on a 5-point scale: 1, the structure is identical; 2, the structure is identical but not well delineated; 3, the structure is still fully identical in all its parts; 4, the structure is well delineated; 5, the structure is very well delineated [21].

For quantitative analysis, image quality was assessed quantitatively by measuring attenuation and image noise. The latter was estimated by measuring the standard deviation Hounsfield units (HU) of circular regions of interest (ROIs) placed in three regions on a 0.5 mm axial section (Fig. 1). The ROIs were analysed

for 40 patients on an Aquilion Prime console by the same radiologist.

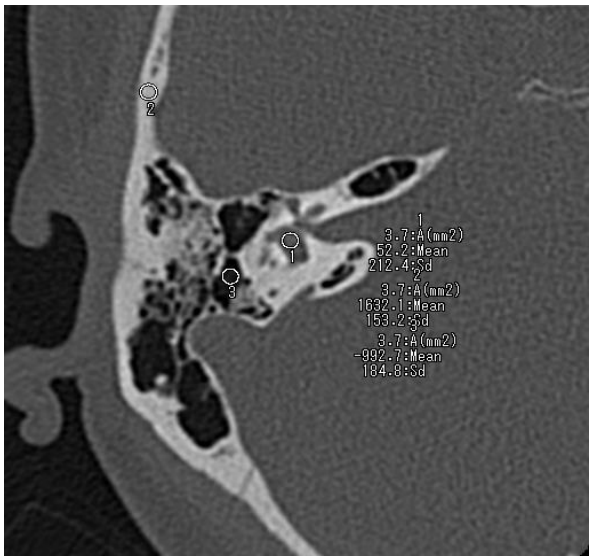

Figure 1. Hounsfield units (HU) and image noise (standard deviation of the attenuation value) measured in three different regions of interest (ROIs). ROIs were placed into Vestibule (1), temporal bone (2), and mastoid (3).

Statistical analysis

The image quality scores from the qualitative analysis were averaged to give an overall image quality score for each series. Then, The Mann Whitney signed-rank test was used to compare the image quality obtained for the two protocols. The test was also used to compare doses according to scanning techniques. P-values below 0.05 are considered statistically significant.

Results

The first group is composed of 20 patients (8 males, 12 females) with an average age of 55.9 years and a CT of HMCT120-kVp was applied. The second group included 20 patients (9 males, 11 females) with an average age of 58.15 years, a CT of VMCT135-kVp was practiced. As a result, there are no significant differences between the two groups in terms of average age and acquisition lengths. In contrast, the mean DLP and effective dose for the VMCT135-kVp protocol were significantly lower than for the HMCT120-kVp protocol ($p < 0.001$), respectively, with an averaged decrease in effective dose of 61.5% (Table 1). The effective radiation doses using VMCT135-kVp protocol scans were approximately 1.73–5.6 times lower even compared with those of literature-based protocols (Table 1).

In the quantitative assessment of image quality, the mean density values for the vestibule and bone were significantly lower in the VMCT135-kVp than in the HMCT120-kVp ($p <0.05$). In contrast, there was no significant difference in area of circular regions of interest (ROI) and image noise averages between the two protocols (Table 2). Regarding the qualitative assessment ,the analysis showed that the image quality scores for the Tympanic Membrane, was significantly lower in both protocols, and the image score for the Tensor Tympani Muscle was significantly lower in the HMCT120-kVp with regards to VMCT135-kVp ($p = 0.022$) as shown in Table 3. There were no statistically significant differences in the mean image quality frequencies (score) between the two protocols. Score 4 was chosen most frequently by 51% for VMCT135-kVp and 50% for HMCT120-kVp. While score 2 was very rarely chosen by 3.4% for HMCT120-kVp and 2.5% for VMCT135-kVp. None of the structures get a score of 1 for both protocols. The mean frequencies of the qualitative scores of the images are shown in Figure 3.

Table 1. Effective doses using conventional HMCT120-kVp and VMCT135-kVp protocols compared to literature-based effective doses.

	HMCT120-kVp protocol	VMCT135-kVp Protocol	C.R. Kim et al 2018[b] [22]	Daichi Noto et al 2015[b] [23]	Lutz et al 2007[b](standard protocol) [19]	Lutz et al 2007[b](low dose protocol) [19]
kVp	120	135	150	140	120	120
mAs	100	75	169.73 ± 2.83[a]	160	180	140
DLP(mGy.cm)	186.4 ± 4.3[a]	69.6 ± 2.5[a]	85.61 ± 8.34[a]	N/A	N/A	N/A
D_{eff} (mSv)	0.39 ± 0.05[a]	0.15 ± 0.01[a]	0.26 ± 0.26[a]	0.84	0.61 ± 0.08[a]	0.31 ± 0.12[a]

[a] Data are the mean ± standard deviation.
[b] Indicates literature-based effective doses.

Table 2. Objective perceptibility of the image: Comparison between HMCT120-kVp and VMCT135-kVp.

Structure parameter	HMCT120-kVp (n=20)	VMCT135-kVp (n=20)	P-value
Vestibule			
Area of ROI (mm2)	3.01 ± 1.04	3.31 ± 0.95	0.383
Attenuation, HU	74.73 ± 12.58	66.25 ± 13.10	0.040[b]
Noise, HU	152.91 ± 42.17	155.96 ± 38.18	0.808
Mastoid [a]			
Area of ROI (mm^2)	2.65 ± 0.73	3.03 ± 0.66	0.134
Attenuation, HU	951.79 ± 74.76	980.83 ± 55.38	0.123
Noise, HU	134.43 ± 53.39	142.52 ± 46.44	0.787
Temporal Bone			
Area of ROI (mm2)	3.16 ± 0.85	3.36±1.04	0.703
Attenuation, HU	1721.73 ± 123.38	1634.23±76.01	0.016[b]
Noise, HU	165.92 ± 46.73	205.30±60.66	0.051

[a] Due to negative HU values, amount of CT density value is given.
[b] Statistical significance.

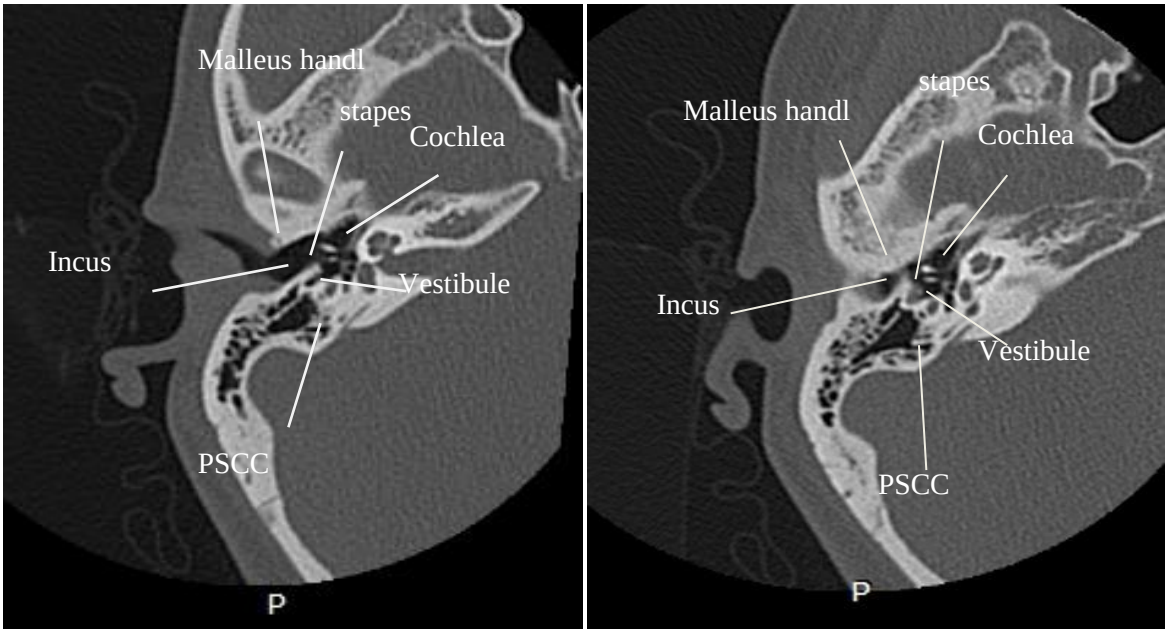

Figure 2. Axial CT image using VMCT135-kVp (Right) and HMCT120-kVp Protocol (Left) of a normal right temporal bone.

Table 3. Subjective image conspicuity: Comparison between the HMCT120-kVp and the VMCT135-kVp Protocol.

Structure	HMCT120-kVp (n=20)	VMCT135-kVp (n=20)	P-value
Jugular forman	4.5±0.51	4.7±0.47	0.202
Formen ovale	4.2±0.61	4.6±0.50	0.038[b]
Vidian Canal	3.8±0.77	4.3±0.80	0.051
Tympanic Membrane	2.4±0.50	2.6±0.50	0.212
Petrous internal carotid artery (ICA)	4.4±0.50	4.2±0.49	0.173
Cochlear Promontory	4.2±0.41	4.0±0.46	0.162
Basal Turn Cochlea	4.3±0.66	4.2±0.41	0.437
Cochlear Aqueduct	4.2±0.61	4.0±0.45	0.227
Mastoid	4.9±0.31	5.0±0.00	0.152
Mastoid Segment Facial Nerve	3.3±0.65	3.0±0.66	0.148
Incudo stapedial Joint	3.1±0.55	3.2±0.77	0.546
Incus Long Process	3.0±0.46	3.4±0.50	0.015[b]
Incus Short Process	3.5±0.51	4.0±00	0.00031[b]
Rond Window Niche	3.4±0.50	3.7±0.66	0.143
Apical Turn Cochlea	3.8±0.41	4.2±0.61	0.023[b]
Middle Turn Cochlea	4.2±0.61	4.5±0.51	0.123
Sinus Tympani	3.8±0.41	3.8±0.41	1.000

Structure	HMCT120-kVp (n=20)	VMCT135-kVp (n=20)	P-value
Jugular forman	4.5±0.51	4.7±0.47	0.202
Formen ovale	4.2±0.61	4.6±0.50	0.038[b]
Vidian Canal	3.8±0.77	4.3±0.80	0.051
Tympanic Membrane	2.4±0.50	2.6±0.50	0.212
Petrous internal carotid artery (ICA)	4.4±0.50	4.2±0.49	0.173
Cochlear Promontory	4.2±0.41	4.0±0.46	0.162
Basal Turn Cochlea	4.3±0.66	4.2±0.41	0.437
Cochlear Aqueduct	4.2±0.61	4.0±0.45	0.227
Mastoid	4.9±0.31	5.0±0.00	0.152
Mastoid Segment Facial Nerve	3.3±0.65	3.0±0.66	0.148
Incudo stapedial Joint	3.1±0.55	3.2±0.77	0.546
Incus Long Process	3.0±0.46	3.4±0.50	0.015[b]
Incus Short Process	3.5±0.51	4.0±00	0.00031[b]
Rond Window Niche	3.4±0.50	3.7±0.66	0.143
Apical Turn Cochlea	3.8±0.41	4.2±0.61	0.023[b]
Middle Turn Cochlea	4.2±0.61	4.5±0.51	0.123
Sinus Tympani	3.8±0.41	3.8±0.41	1.000
Pyramidal Eminence	3.3±0.47	3.9±0.31	0.00031[b]
Labyrinthine Nerve	3.5±0.51	3.4±0.50	0.530
Facial Recess	3.2±0.89	4.1±0.31	0.00023[b]
Stapes	3.2±0.61	3.4±0.82	0.238
Malleus Head	4.1±0.55	4.4±0.68	0.100
Malleus Handle	4.0±0.46	3.8±0.41	0.162
MalleoIncudal Joint	3.7±0.47	3.6±0.50	0.513
Modiolus	4.1±0.55	3.8±0.41	0.064
Korner Septum	4.3±0.66	4.0 ±0.0	0.148
Geniculate Ganglion	3.6±0.50	3.8±0.41	0.173
Vestibule	4.4±0.50	4.6±0.50	0.212
Vestibule Aqueduct	4.0±0.46	3.9±0.72	0.565
Mastoid Antrum	4.7±0.47	4.4±0.50	0.060
Aditus and antrum	4.4±0.50	4.5±0.51	0.530
Internal Auditory Canal (IAC)	4.5±0.51	4.6±0.50	0.530
Petrous Apex	4.6±0.50	4.4±0.50	0.212
Sigmid Sinus	4.3±0.66	4.3±0.66	1.000
Eustachian Tube	4.0±0.46	4.2±0.61	0.227
Lateral semicircular canal (LSCC)	4.5±0.51	4.4±0.50	0.530
Superior semicircular canal (SSCC)	4.6±0.50	4.5±0.51	0.530
Posterior semicircular canal (PSCC)	4.3±0.47	4.4±0.50	0.513
Occipito Mastoid Suture	4.3±0.66	4.3±0.66	1.000
Tympanic Segment Facial Nerve	3.1±0.55	3.2±0.62	0.563
Tensor Tympani Muscl	2.7±0.47	3.2±0.77	0.022[b]
Cochlea	4.5±0.51	4.7±0.47	0.202
Clivus	4.2±0.41	4.8±0.41	0.00017[b]
Scutum	4.2±0.41	4.8±0.41	0.00018[b]
Prussak Space	4.7±0.47	4.3±0.66	0.042[b]
Petro Occipital Synchondroses	4.2±0.77	4.4±0.68	0.409
Tensor Tympani Tendon	3.3±0.80	3.6±0.68	0.166
Tegment Tympani	4.1±0.55	4.0±0.46	0.520
Arcuate Eminence	3.9±0.72	4.2±0.41	0.125
Oval Window	3.7±0.65	3.7±0.47	0.850
Jugular Tubercule	4.5±0.51	4.7±0.47	0.202
Hypoglossal Canal	4.9±0.31	4.9±0.31	1.000

[b] Statistical significance.

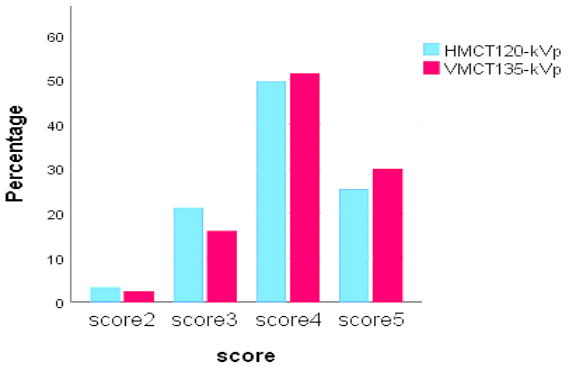

Figure 3: Bar chart of the information in Table 3. Comparison of the frequency (percentage) of the image perceptibility scores between the two CT scans protocols.

Discussion

One of the main advantages of the volumetric mode is the significant reduction in CT image acquisition time compared to the helical mode [24]. On the one hand, this decrease in acquisition time could be beneficial for uncooperative individuals and children to avoid the risks and inconvenience of sedation and general anesthesia [25]. On the other hand, artifacts related to the movement of the patient can theoretically lead to repetitive scans implying additional radiation exposure [20]. In this context, our study investigates the possibility to optimize the received dose while maintaining the image quality of temporal bone imaging using volumetric mode, an area of 40 mm in the z-axis can be covered in only 0.5 seconds at a time and without table translation during acquisition, compared to 1.42 seconds in the helical mode.

The 128-slice CT scan with the single-shot technique significantly reduced radiation exposure, as reported by Schwab et al [20], but this dose reduction has a compromise in spatial resolution, the acquisition collimation was 0.75 mm, the image evaluation section thickness was 0.8 mm. However, we achieved short acquisition time and high spatial resolution by superimposing reconstructions of 0.5 mm slices thickness every 0.25 mm. In another study, HC Bauknecht [13] used a cadaverous head phantom by testing several protocols. They obtained an irradiation dose of 0.47 mSv with the low-dose protocol compared to the standard protocol and also demonstrated that both techniques provided comparable image quality. Furthermore, in our study, the radiation dose obtained with VMCT135-kVp was 0.15 mSv.

The temporal bone is ideally suited for low-dose CT, because all bony structures are surrounded by an air component that produces high intrinsic contrast [26]. A previous study reported that the normal anatomy of the temporal bone in young children could be adequately assessed with a significant reduction in radiation exposure. As a result of this study, image quality was assessed qualitatively using a 5-point scale, and no quantitative method was performed [21]. In our study, we applied both qualitative and quantitative methods to assess image quality in both protocols.

Our study confirms that there is no significant difference in image noise between the two protocols and that image noise was lower in the HMCT120-kVp helical mode than in the VMCT135-kVp volumetric mode, but was within an acceptable range for the evaluation of ear structures. The HU attenuation was lower for the vestibule and bone, and was higher for the mastoid in VMCT135-kVp than in HMCT120-kVp, because as the beam energy increases, the radiation transmission increases aswell and simultaneously the attenuation coefficients decrease. Thus, the number of tissues less dense than water increases and the number of tissues more dense than water decreases [19].

In terms of image quality diagnostic, no significant differences are observed regarding statistical comparison of HMCT120-kVp with the VMCT135-kVp used in this study, more anatomical structures were sufficiently visible. Even though the tube current-time product (mAs) is low with the VMCT135-kVp, the image quality is interpretable due to image noise reduction by the iterative reconstruction [23]. On the other hand, there was a significant difference in 10 of the 53 structures (19%), such as the Incus, Apical Turn Cochlea, Pyramid Eminence, Facial Recess, Clivus, Scutum, Prussak Space, Petro-occipital synchondrosis, or Form ovale, which were imaged without significant loss of image quality information, except for the Tensor Tympani Muscle, which was significantly worse assessed by HMCT120-kVp. In particular, the frequency of scores 4 and 5, indicating high image quality, was higher for the VMCT135-kVp than for the HMCT120-kVp (51.8% and 30% for the VMCT135-kVp versus 50.2% and 24.1% for the HMCT120-kVp), score 3 was 14% for VMCT135-kVp and 21.3% for HMCT120-kVp, However, the frequency of score 2, indicating poor image quality, was very low for both procedures (<2%).

Conclusion

Volumetric mode VMCT135-kVp on an 80-detector scanner results in a lower dose to temporal bone organs compared to helical mode HMCT120-kVp. The shorter acquisition time of VMCT135-kVp may reduce the need for sedation in children and uncooperative patients, as well as the received dose in radiation-sensitive organs at risk, such as the optic nerve, lens, or parotid gland. The image quality was assessed in terms of a 5-point score basis attributed by an experimental radiologist; the highest image quality gets the highest score. The analysis has been demonstrated comparable image quality scores for both acquisition modes; the images were of high quality as the higher frequency was observed for score 4; with relatively low mAs and short exposure time compared to the values reported in the literature. This study has shown and approved that optimizing the dose exposure while maintaining a good image quality is possible and achievable using the VMCT135-kVp. This contribution aims to enhance the

radiology imaging protocol and guarantee the patient and staff radiation protection.

References

1. Guberina N, Dietrich U, Arweiler-Harbeck D, Forsting M, Ringelstein A. Comparison of radiation doses imparted during 128-, 256-, 384-multislice CT-scanners and cone beam computed tomography for intra-and perioperative cochlear implant assessment. American journal of otolaryngology. 2017 Nov 1;38(6):649-53.
2. Chen JY, Mafee MF. Computed tomography imaging technique and normal computed tomography anatomy of the temporal bone. Operative Techniques in Otolaryngology-Head and Neck Surgery. 2014 Mar 1;25(1):3-12.
3. Jackler RK, Parker DA. Radiographic differential diagnosis of petrous apex lesions. Otology & Neurotology. 1992 Nov 1;13(6):561-74.
4. Basraoui D, Elatiqi K, Jalal H. computed tomography of the petrous bone: Particularities in children. Advances in Molecular Imaging. 2018 May 29;8(2):15-24.
5. Nauer CB, Zubler C, Weisstanner C, Stieger C, Senn P, Arnold A. Radiation dose optimization in pediatric temporal bone computed tomography: influence of tube tension on image contrast and image quality. Neuroradiology. 2012 Mar;54:247-54.
6. Meyer M, Haubenreisser H, Raupach R, Schmidt B, Lietzmann F, Leidecker C, et al. Initial results of a new generation dual source CT system using only an in-plane comb filter for ultra-high resolution temporal bone imaging. European radiology. 2015 Jan;25:178-85.
7. Unlu E, Okur N, Acay MB, Kacar E, Ozdinc S, Balcik C, et al. The prevalence of incidentally detected idiopathic misty mesentery on multidetector computed tomography: can obesity be the triggering cause?. Canadian Association of Radiologists' Journal. 2016 Aug;67(3):212-7.
8. International Commission on Radiological Protection. Recommendations of the ICRP. ICRP publication 26. Ann. ICRP. 1977;1(3).
9. van der Molen AJ, Geleijns J. Overranging in multisection CT: quantification and relative contribution to dose—comparison of four 16-section CT scanners. Radiology. 2007 Jan;242(1):208-16.
10. Christner JA, Zavaletta VA, Eusemann CD, Walz-Flannigan AI, McCollough CH. Dose reduction in helical CT: dynamically adjustable z-axis X-ray beam collimation. American journal of roentgenology. 2010 Jan;194(1):W49-55.
11. Schilham A, van der Molen AJ, Prokop M, de Jong HW. Overranging at multisection CT: an underestimated source of excess radiation exposure. Radiographics. 2010 Jul;30(4):1057-67.
12. Cody DD, Mahesh M. Technologic advances in multidetector CT with a focus on cardiac imaging. Radiographics. 2007 Nov;27(6):1829-37.
13. Bauknecht HC, Siebert E, Dannenberg A, Bohner G, Jach C, Diekmann S, et al. Image quality and radiation exposure in 320-row temporal bone computed tomography. Dentomaxillofacial Radiology. 2010 May;39(4):199-206.
14. Tada A, Sato S, Masaoka Y, Kanazawa S. Imaging of the temporal bone in children using low-dose 320-row area detector computed tomography. Journal of Medical Imaging and Radiation Oncology. 2017 Aug;61(4):489-93.
15. Podberesky DJ, Angel E, Yoshizumi TT, Toncheva G, Salisbury SR, Brody AS, et al. Comparison of radiation dose estimates and scan performance in pediatric high-resolution thoracic CT for volumetric 320-detector row, helical 64-detector row, and noncontiguous axial scan acquisitions. Academic Radiology. 2013 Sep 1;20(9):1152-61.
16. Jafari S, Karimi M, Khosravi H, Goodarzi R, Pourkaveh M. Establishment of diagnostic reference levels for computed tomography scanning in hamadan. Journal of Biomedical Physics & Engineering. 2020 Dec;10(6):792.
17. Muhammad NA, Kayun Z, Abu Hassan H, Wong JH, Ng KH, Karim MK. Evaluation of organ dose and image quality metrics of pediatric CT chest-abdomen-pelvis (CAP) examination: an anthropomorphic phantom study. Applied Sciences. 2021 Feb 25;11(5):2047.
18. Niu YT, Mehta D, Zhang ZR, Zhang YX, Liu YF, Kang TL, Xian JF, Wang ZC. Radiation dose reduction in temporal bone CT with iterative reconstruction technique. American journal of neuroradiology. 2012 Jun 1;33(6):1020-6.
19. Lutz J, Jäger V, Hempel MJ, Srivastav S, Reiser M, Jäger L. Delineation of temporal bone anatomy: feasibility of low-dose 64-row CT in regard to image quality. European radiology. 2007 Oct;17:2638-45.
20. Schwab SA, Eberle S, Adamietz B, Kuefner MA, Kramer M, Uder M, and et al. Comparison of 128-section single-shot technique with conventional spiral multisection CT for imaging of the temporal bone. American Journal of Neuroradiology. 2012 Apr 1;33(4):E55-60.
21. Nauer CB, Rieke A, Zubler C, Candreia C, Arnold A, Senn P. Low-dose temporal bone CT in infants and young children: effective dose and image quality. American journal of neuroradiology. 2011 Sep 1;32(8):1375-80.
22. Kim CR, Jeon JY. Radiation dose and image conspicuity comparison between conventional 120 kVp and 150 kVp with spectral beam shaping for temporal bone CT. European Journal of Radiology. 2018 May 1;102:68-73.
23. Noto D, Funama Y, Kitajima M, Utsunomiya D, Oda S, Yamashita Y. Optimizing radiation dose by varying age at pediatric temporal bone CT. Journal of applied clinical medical physics. 2015 Jan;16(1):311-8.
24. Bauknecht HC, Siebert E, Dannenberg A, Bohner G, Jach C, Diekmann S, and et al. Image quality and radiation exposure in 320-row temporal bone computed tomography. Dentomaxillofacial Radiology. 2010 May;39(4):199-206.
25. Kaste SC, Young CW, Holmes TP, Baker DK. Effect of helical CT on the frequency of sedation in pediatric patients. AJR. American journal of roentgenology. 1997 Apr;168(4):1001-3.
26. Husstedt HW, Prokop M, Dietrich B, Becker H. Low-dose high-resolution CT of the petrous bone. Journal of Neuroradiology= Journal de Neuroradiologie. 2000 Jun 1;27(2):87-92.